Visualization of the UF Polarized Layer by Holographic Interferometry

M. J. Fernández-Torres, F. Ruiz-Beviá, and J. Fernández-Sempere
Dept. de Ingeniería Química, Universidad de Alicante, E-03080 Alicante, Spain

M. López-Leiva
Dept. of Food Engineering, Lund University, S-221 00 Lund, Sweden

The technique of holographic interferometry used to visualize the ultrafiltration membrane surroundings makes it possible to visualize solute retention and verify whether or not there is cake formation on the membrane surface during the ultrafiltration of bovine serum albumin (BSA) protein using a polyethersulfone membrane. The experimental results indicate the presence of a gelatinous mass or a filter cake during BSA ultrafiltration using the membrane mentioned. This was shown by the small concentration profile obtained from the interferometric information and from direct observation of the membrane environs when the pump stopped, which showed the appearance of a gelatinous material adjacent to the membrane.

Introduction

Ultrafiltration is a pressure-driven technique that uses very fine semipermeable membranes where filtration takes place at molecular level. In this way, small substances dissolved in the liquid pass through the membrane, while large molecules, colloidal particles, and the solids in suspension are retained. This method allows larger macromolecules to be separated from smaller species, and it is therefore a very useful technique in fields such as pharmacy, biology, and food technology. The transmembrane volumetric flux obtained during ultrafiltration of molecular solutions is usually much smaller than that obtained with pure solvent (depending on the membrane material, the solute concentration, etc.). This reduction has been attributed to the phenomenon of concentration polarization—the buildup of rejected solute in the boundary layer near the membrane surface. Such a build-up concentration generates a diffusive flow back to the bulk of the feed. If steady-state conditions are reached, the convective solute flow to the membrane surface is balanced by the solute flux through the membrane plus the diffusive flow from the membrane surface to the bulk.

The mechanism by which flux reduction occurs has been variously thought to be (a) a reduction in the driving force resulting from the increased osmotic pressure at the membrane surface, or (b) the formation of the so-called gel layer, which offers a hydraulic resistance in addition to that of the membrane. In the first case, solute molecules retained by the membrane remain in solution and the established concentration profile greatly increases its slope. In the second case, the concentration profile has a smaller slope because part of the retained solute molecules are not in solution, but form a gel. It should be pointed out that ultrafiltration literature uses the term "gel" in the sense of coagulation, aggregation–precipitation, of a colloidal macromolecular solution, but not in the strict sense of the term "gel," which then means voluminous network structures that possess a certain degree of stiffness (gel strength). Consequently, in recent works on bovine serum albumin (BSA) ultrafiltration, some authors prefer to use the filter-cake concept instead of the gel-layer concept (e.g., Nakakura et al., 1997; Bowen and Ahmad, 1997; Mukai et al., 1997). The solute accumulation in the filter cake gives rise to a flat concentration profile. Figure 1, which is an adapted figure from Noble and Stern (1995), shows the concentration polarization profiles according to film theory, gel layer model, and cake-filtration theory.

When ultrafiltering protein BSA, there are discrepancies between different authors about which of the previous mechanisms is predominant. Vilker et al. (1981b) and Boulanouar et al. (1996) claim that an insoluble gel-type layer is not formed at the membrane surface during BSA ultrafiltration because at that point in their experiments the solute concentration did not reach the limiting concentration correspond-

Correspondence concerning this article should be addressed to M. J. Fernández-Torres.

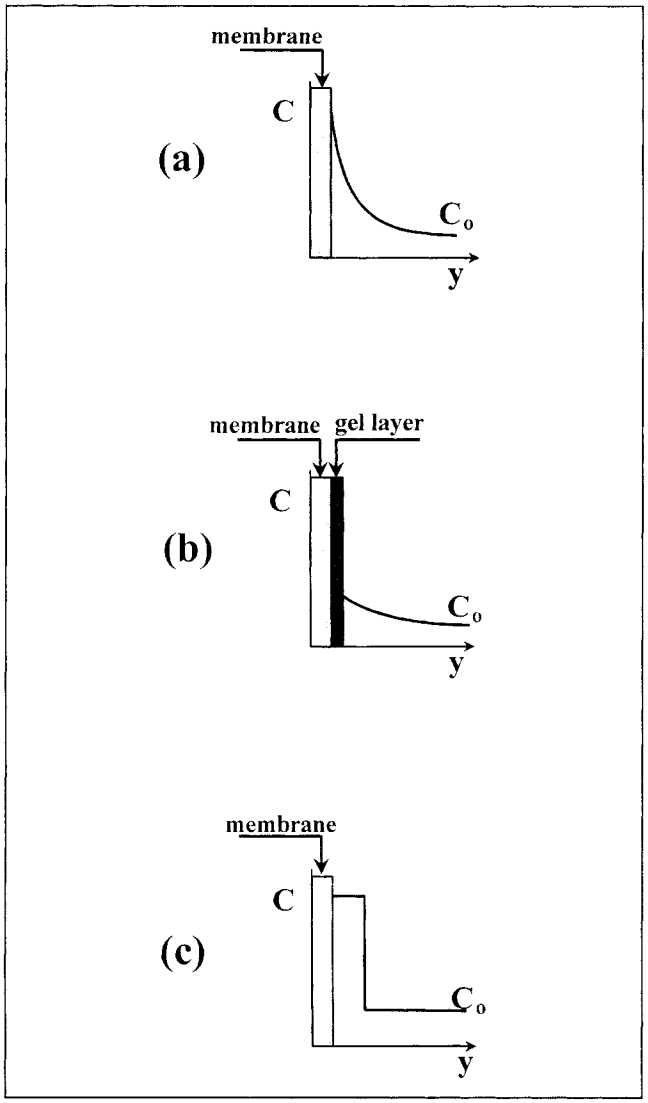

Figure 1. Concentration profiles due to concentration polarization: (a) film theory; (b) gel-layer model; (c) cake filtration theory.

ing to solubility or gelification of BSA. In the literature, the BSA solubility near the isoelectric point (pH = 4.7) is estimated to be 610 kg/m^3 from studies of BSA in water (MacRitchie, 1973) and to be 585 kg/m^3 from viscosity studies (Kozinski and Lightfoot, 1972). However, Matthiasson (1984) regards it as possible that a BSA gel could be formed at a concentration below the limiting concentration due to the interactions between the macrosolute and the membrane surface as well as due to the protein aggregates becoming compact as a consequence of the pressure applied during the ultrafiltration process. Dynamic mathematical ultrafiltration models based on the description of the particle–particle interactions within the filter cake for charged inorganic colloids (Bowen and Jenner, 1995) and proteins (Bowen and Williams, 1996) have been developed. These models allow quantitative prediction of the rate of filtration controlled by specific cake resistance. Recently, Nakakura et al. (1997), using electrical conductivity measurements of protein solutions, claimed that filter cakes formed from protein solutes behave as highly compressible cakes. In any case, the actual mechanism of the fouling that occurs due to protein adsorption, aggregation, and denaturation is not well understood, as admitted by Nabe et al. (1997).

The little information that is known about the polarized layer is the reason for the previous discrepancies. This lack of knowledge is mainly due to the experimental difficulties associated with making nondestructive concentration profile determinations within a very thin layer. Most of the studies made to experimentally determine concentration profiles during membrane processes have been related to reverse osmosis. Because the solute accumulated in the polarized layer in this case is usually a salt, concentration gradients can be measured using techniques based on the variation of solution conductivity with concentration. For instance, Liu and Williams (1970) and Hendricks and Williams (1971) used conductivity microelectrodes specifically designed for this purpose. Classic interferometry has been used to study the polarized layer in reverse osmosis (Johnson, 1974; Mahlab et al., 1978).

Few experimental studies have been conducted to quantify concentration profiles during ultrafiltration of proteins. Evidently, in this case conductivity techniques are not useful and optical methods are therefore preferred. Vilker et al. (1981a,b) are the pioneers in this type of study. They employed the shadowgraph technique to study the concentration profiles in the concentration polarized layer in the ultrafiltration of BSA. This kind of study is very important due to the difficulties encountered in the study of a very narrow layer. Using this technique, they were able to obtain 13 concentration profiles for 11 different experiments carried out under different conditions. The shadowgraph method is based on the principle that light is deflected when passing through a medium with a continuously varying refractive index. The refractive-index profile above a membrane (and the related concentration profile) is obtained from measurements of the light deflection caused by such a refractive-index gradient. This technique requires a large refractive-index gradient in order to minimize deflection measurement errors. To do this, the authors worked with a high feed concentration and allowed the batch ultrafiltration to run for at least 9 h. In one experiment, however, with high feed concentration (158 kg/m^3), they obtained two concentration profiles after relatively short times: 33 and 88 min. The shadowgraph technique has its limitations due to the following factors: first, the exact membrane position must be known in order to measure deflections of the light that passes through the concentration polarization layer. This requires a careful alignment of the optical system, and a correct parallelism between the transparent walls of the module. Second, the module walls must be made of quality glass, and be of uniform thickness.

McDonogh et al. (1992, 1995) used another experimental optical method to directly measure the concentration profile by means of the electronic diode array microscope (EDAM) technique. For the ultrafiltration run the authors employed blue dextran and BSA protein dyed with coomassie brilliant blue, since this technique is subjected to solute adsorption in IR. In the case of dead-end ultrafiltration experiments, McDonogh et al. show that the extent of polarization for BSA is less than for dextran. The concentration near the membrane and the extent of the polarized layer both increase with time.

The relative increases for BSA are much smaller than those for dextran, and the time taken for the polarized layer development is much longer (up to 18 h).

Ethier and Lin (1992) used differential refractometry to measure the polarization development in the filtration of hyaluronan solutions in a dead-end UF flow cell. In subsequent studies Gowman and Ethier (1997a,b) described the technical aspects of a redesigned system based on the preliminary work of Ethier and Lin (1992). The physicochemical properties of the bipolymer used (hyaluronan) were quite different from those of BSA.

In this article, in order to obtain better knowledge of the phenomena taking place on the membrane surface, a microscopic holographic interferometric method was developed to monitor in real time the solute retention during protein ultrafiltration in an unstirred cell. In this way, the evolution of solute concentration can be visualized as interference fringes. Holographic interferometry can be defined as the interferometric comparison of two or more waves, at least one of which is holographically reconstructed (Vest, 1979). This technique has been used before to study diffusion, both in liquid and in gel systems (Ruíz et al., 1985a,b, 1989, 1995; Fernández et al., 1996). The method visualizes changes in the refractive index (due to changes of concentration) as interference fringes, and therefore can be used to study the concentration polarized layer formation in ultrafiltration. Furthermore, since the technique is differential in time, and the two waves that interfere are separated temporally rather than spatially, it can be used to follow the evolution of the system under study, with time. Holographic interferometry presents some advantages over classic interferometry: it is simpler, only one cell is needed (because the comparison is between two images of the same cell obtained at different times), there is no need for windows of high optical quality on the ultrafiltration cell, and the inhomogeneities in the windows of the cell do not cause perturbations in the measurements. In this article, the tubular body of a microscope was fitted to a lensless video camera in order to holographic interferometrically record the evolution of the ultrafiltration process. It has been previously said that classic interferometry has been used to study the polarized layer in reverse osmosis (Johnson, 1974; Mahlab et al., 1978) but not in ultrafiltration. Clifton and Sánchez (1979) successfully applied holographic interferometry to study the polarized layer during the electrodialysis of KCl aqueous solutions; however, they had difficulties when a 0.05% synthetic polymer solution (polyvinyl pyrrolidone) was ultrafiltered. They could not visualize interference fringes when the polarized layer was being formed, although later when the pump was stopped, fringes were observed. This was because after the flow was stopped, the solute contained in the boundary layer was allowed to diffuse into the bulk of the solution, making the observation of interference fringes possible.

In addition to extending the use of holographic interferometry to the study of mass-transfer processes through membranes, the objectives of this research are to obtain the evolution of concentration profiles during protein ultrafiltration in an unstirred cell and to detect the presence of a cake layer during ultrafiltration. These points have great relevance when designing complete models of BSA ultrafiltration. The results of the present study show that a filter cake is formed during BSA ultrafiltration.

Materials and Methods

Ultrafiltration module

To adapt the ultrafiltration system to the holographic interferometry requirements, a special ultrafiltration module was designed to permit the observation of the limit between membrane and solution through transparent windows. Figure 2 shows the module (open) used, which works in batch filtration. The upper part is made of stainless steel, whereas the bottom part is made of Teflon. Screws are used to mount the module in place. To avoid using an O-ring to press the membrane between the parts of the module, the bottom part (Figure 2) was designed with a raised membrane support to observe the membrane–solution zone, where the concentration polarization phenomenon takes place, through the window. The channel is 0.12 m long, 0.02 m wide, and 0.005 m high. The membrane is fixed to the bottom part of the module by gluing the perimeter to the raised support. The usable membrane surface, glued above the raised support, is 0.10 m long $\times$0.01 m wide. Two tests were carried out to check the membrane tightness: (1) measurement of water permeate flux prior to the ultrafiltration experiment—the water flux was determined by weight, which had to be in the range given by the manufacturer—and (2) measurement of the concentration of BSA in the permeate after the ultrafiltration experiment—this concentration had to be much less than the feed concentration. The quantitative BSA determination was made with a spectrophotometer (Shimadzu UV-120-01) at 595 nm, after reacting with Coomassie Brilliant Blue G-250 (Merck) (Bradford, 1976).

Although our ultrafiltration module can work in cross-flow conditions, all the experiments presented in this article have been carried out in batch conditions. The dead end of the circuit valve in Figure 2 was closed during the experiment and was only open for filling the module with BSA solution, in order to eliminate air present in the system.

The whole ultrafiltration system in Figure 3 consists of: feed tank (1); water tank (2); 3-way valve (3); pump (4) (Micropump 200), which is installed outside the optical bank to avoid vibrations; thermometer (5); pressure gauges (6); ultrafiltration module (7), which is installed in a vertical position to avoid bubble retention; circuit valve dead end (8); permeate collector vessel (9); balance (10); and computer (11).

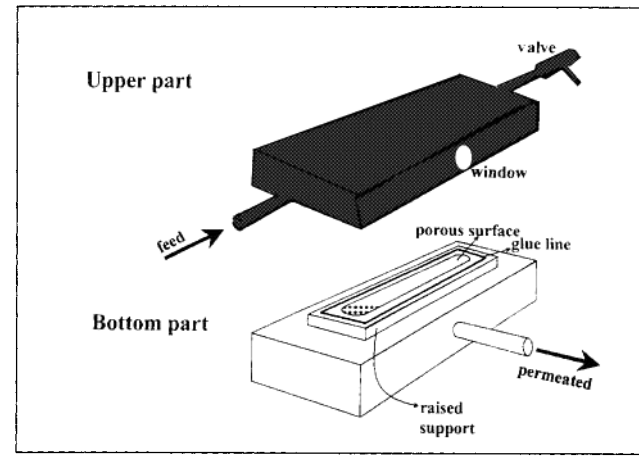

Figure 2. Ultrafiltration module employed.

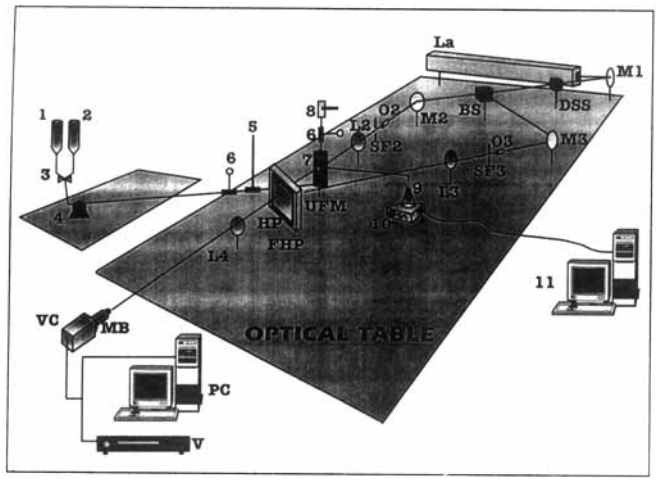

Figure 3. Optical and ultrafiltration set-ups.

La: He–Ne laser. DSS: Digital shutter system. BS: Variable attenuator/beam splitter. M_i: Mirrors. L_i: Lenses. O_i: 10× microscope objective lenses. SF_i: spatial filters. UFM: Special ultrafiltration module with transparent windows. FHP: Film holder/processor. HP: Holographic plate. MB: Tubular body of a microscope adapted to the video camera. VC: Lensless video camera. PC: computer. V: Videocassette recorder. 1: Feed tank. 2: Water tank. 3: Three-way valve. 4: Pump. 5: Thermometer. 6: Pressure gauges. 7: Ultrafiltration module. 8: Dead end of circuit valve. 9: Permeate collector vessel. 10: Balance. 11: Computer.

Holographic interferometry system

The optical setup (joined to the ultrafiltration system) is shown in Figure 3: a He–Ne laser (La) (Spectra Physics, model 127, 35 mV) emits coherent light at 632.8 nm. The laser beam, which can be interrupted by a digital shutter system (DSS) (Newport Corporation, model 845 HP), is divided in two—the reference beam and the object beam—by a variable attenuator/beam splitter (BS) (Newport Corporation model 930-63). The reference beam is directed to the holographic plate (HP) (Agfapan 25 from AGFA) by means of a mirror, whereas the object beam passes through a special ultrafiltration module (UFM) with transparent windows and impinges on the holographic plate. A film holder/processor (FHP) (Newport Corporation model 550) is used to chemically process the holographic plate and allows the plate to be held in place during the entire experiment to avoid plate shifting. A horizontal/vertical measuring microscope (Ealing, model 11-3357) was fitted to a lensless video camera (VC) (Sony CCD, model AVC-D7CE) in order to continuously record the experiments. This setup allows the study of different zones through the transparent window of the ultrafiltration module. The optical system is placed on an optical table (Newport Corporation M-RS-48-8) provided with three isolated vibration legs (Newport Corporation XLB2A-28T). The experimental apparatus is placed in a room at constant temperature, 25 ± 0.2°C.

Materials

BSA (SIGMA, A 7906) was used in all the experiments. Aqueous solutions were prepared using twice-distilled water. All the solutions were 0.15 M in NaCl (PANREAC) to establish the ionic strength and 0.02% in NaN_3 (PANREAC) to prevent bacterial growth. Fresh BSA feed solution was prepared at the beginning of each experiment. The resulting pH was around 6.8 in all cases and was not changed.

All the experiments were performed with the same type of polyethersulfone (UF-PES-4/PET 100 from Kalle) membrane. This membrane has high chemical stability and high hydrophilicity, which is ideal for the ultrafiltration of solutions that normally cause fouling problems.

Experimental methodology to obtain interferograms

At least 12 h after gluing the membrane to the bottom part of the module, the upper part is put into place. Then the module is mounted and placed on the optical table. Pure water is pumped through the ultrafiltration system for 30 or 40 min, until the permeate flux becomes constant. Measurement of the water flux is made in a continuous way by using a balance connected to a computer. Afterwards the water can be drained out of the ultrafiltration system and replaced by the BSA feed solution.

In order to carry out the holographic interferometric study, two states of the ultrafiltration process must be compared: one is the reference state and the other is the state corresponding to the evolution of the concentration polarization phenomenon. The reference state chosen corresponds to the ultrafiltration module, which is filled with BSA solution and allowed to rest. Once the ultrafiltration module is filled with BSA, with the pump (element 4, Figure 3) disconnected, the hologram is recorded on the holographic plate (HP). To do this, the room is kept in darkness and the path of the laser beam is blocked by means of the digital shutter system (DSS). The holographic plate is placed in the film holder/processor (FHP) and the DSS is opened, impinging the object beam (after passing through the ultrafiltration module) and the reference beam on HP. With the room still in darkness, the plate is chemically processed in the same film holder/processor (the holographic plate is not moved from its original position) to avoid modifications due to plate shifting. The processed holographic plate is the hologram. After that, the laser beam is again allowed to pass through the holographic plate. Later, when the pump is connected ($t = 0$) and the laboratory lights switched on, the ultrafiltration process can be followed (real-time holographic interferometry), as it takes place as a succession of interferometric images (interferograms). During the ultrafiltration process, BSA molecules reach the membrane surface due to the pressure gradient and remain there because the membrane does not allow them to pass through. Thus, the BSA concentration increases above the membrane surface and a concentration profile appears. This concentration profile results in a refractive index gradient that can be used in holographic interferometry. Therefore, the layer of retained solute formed above the membrane is observed as an interferometric fringe layer. Each interferometric fringe represents a change in the refractive index. Recording the interferograms is carried out continuously by a lensless video camera. As stated previously, the concentration polariza-tion layer develops in a narrow frame, and because of this, microscopic holographic interferometry has been used. The magnifications used are shown in the interferograms. After stopping the pump, the recording of the experiment continues for some time in order to visualize the effect of the polarized layer.

One piece of membrane was reused for some experiments. At the end of each experiment a cleaning procedure was carried out. First, the ultrafiltration module was washed with bidistilled water, then it was cleaned with a 1% P3-Ultrasil 10 (Henkel) solution, at 50–70°C, for at least 60 min until the BSA was removed. Finally, the module was washed with bidistilled water until the detergent was completely eliminated. Usually, the retention membrane coefficient was greater than 95% in all the experiments carried out.

Methodology to quantitatively obtain concentration profiles from interferograms

For those substances in which the refractive index changes when the concentration changes, it is possible to visualize by means of holographic interferometry the concentration profiles as an interferometric fringes pattern. In the case of BSA solutions, there is a linear relation between refractive index and BSA concentration, at least up to 60 g/100 mL (Vilker, 1975).

Through holographic interferometry it is possible to record information concerning the reference state (the hologram) on a photosensitive film. When the ultrafiltration process starts, the laser beam that passes through the module interferes with the reference state recorded on the holographic plate and the resulting image recorded on a video tape is the interferogram containing the interference fringes. A succession of interferograms representing the process is obtained by means of continuous recording on a videotape. In each interferogram, a series of interference fringes appears superimposed on the image of the cell whenever the following condition is satisfied:

$$\Delta n \cdot d = \frac{(2k+1)\lambda}{2}, \qquad (1)$$

where Δn (dimensionless) is the change in refractive index between two adjacent fringes, k is the interference order, λ is the wavelength of the light used (632.8 nm), and d is the thickness of the liquid that the light passes through. In our case, as d remains constant, the formation of a new fringe implies a change in refractive index equal to Δn that corresponds to a change in BSA concentration equal to ΔC.

The process to quantitatively obtain concentration profiles available from the interferograms recorded on the videocassette is as follows:

1. To take note of the original position of the membrane surface before each experiment. We attribute $y = 0$ to this position.
2. To follow the evolution of the recorded experiment, attributing an order number to each fringe that appears: the first fringe, 1; the second, 2; and so on.
3. To freeze one image from the recorded videocassette corresponding to a certain time after the beginning of the experiment.
4. To locate visually on this image the position of the maximum darkness related to each fringe referred to the original position of the membrane surface.
5. To determine Δn from Eq. 1. In our case $\Delta n = 3.164 \times 10^{-5}$.
6. To calculate the corresponding refractive index for each fringe, using the following expression:

$$n = n_o + (\text{order number}) \cdot \Delta n, \qquad (2)$$

where n_o is the refractive index of the initial feed solution whose concentration is C_o. That is to say, a refractive index is attributed to each fringe related to each order number. The first fringe implies one change in the refractive index with respect to that corresponding to the feed solution, the second fringe two changes, and so on.

7. To evaluate the concentration corresponding to each refractive index (n) at the position of the fringe (Vilker, 1975).
8. To plot concentration vs. distance from the membrane.

The process is graphically summarized in Figure 4. It can be seen in the figure that the distance of each fringe from the membrane surface is obtained from one chosen interferogram (Figure 4a). Figures 4b and 4c show pairs of data for each fringe: refractive index or concentrations with distance.

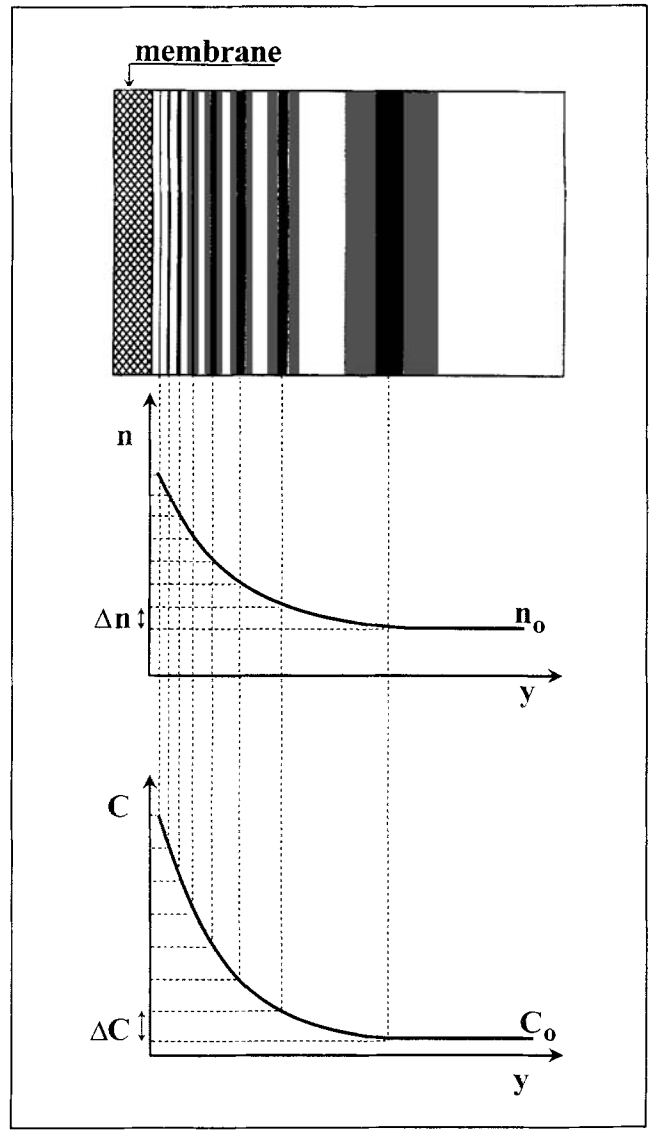

Figure 4. Methodology used to obtain concentration profiles from the interferometric images recorded on the videocassette.

Results and Discussion

Visualization of the polarized layer

In order to visualize the polarized layer, many BSA ultrafiltration experiments were carried out in an unstirred batch module. A continuous, real-time interferometric recording of the experiments was made using a lensless video camera fitted to a tubular microscope body. The reproducibility of the observed behavior was confirmed by repeating several times the ultrafiltration runs at the same conditions (initial feed concentration and transmembrane pressure). All the experiments carried out can be grouped into four categories according to the following approximate operational conditions (C_o, initial feed concentration; ΔP, transmembrane pressure):

- 1st group $C_o = 1$ kg/m^3 and $\Delta P = 1\times10^5$ Pa
- 2nd group $C_o = 10$ kg/m^3 and $\Delta P = 1\times10^5$ Pa
- 3rd group $C_o = 10$ kg/m^3 and $\Delta P = 1.5\times10^5$ Pa
- 4th group $C_o = 50$ kg/m^3 and $\Delta P = 2.2\times10^5$ Pa.

As an example, Table 1 shows the operating conditions corresponding to four experiments, each one representing one of the previously mentioned groups: J_{water} is the volumetric permeate flux with pure water before the start of the ultrafiltration experiment; the a and b values are the parameters in the empirical equation,

$$J = a\exp(-bt), \tag{3}$$

which properly correlates the experimental data during the ultrafiltration process; and R_m is the membrane hydraulic resistance to the flux with pure water, which is calculated as

$$R_m = \Delta P/J_{water}. \tag{4}$$

The visual field indicates the true dimensions of the rectangular zone observed by means of the optical system's video camera–microscope.

The use of microscopic holographic interferometry made it possible to follow the evolution of the interference fringes. The region that can be visualized depends on the objective–ocular combination used in the microscope tubular body. When the whole surface corresponding to the ultrafiltration cell window is visualized, a membrane length of 0.0049 m can be observed. However, to visualize the narrow interference fringes closest to the membrane surface, an appropriate objective–ocular combination must be used, with which the membrane length is observed to be around 0.001–0.002 m (Figure 5). Obviously, since the ultrafiltration module is placed vertically on the optical table, the membrane surface will be visualized as a vertical line.

In an ultrafiltration run, the first interference fringes appear only a few seconds after the pump is switched on. Some minutes later, the number and position of the interference fringes were nearly stable. Figure 6 corresponds to an experiment with $C_o = 50.6$ kg/m^3 and $\Delta P = 2.286\times10^5$ Pa and shows three interferograms at the beginning of the experiment (10, 21, and 42 s, respectively), as well as three other interferograms corresponding to the same experiment, but recorded at a later time (600, 1,200 and 1,800 s). As can be seen, the interference fringes rapidly became stable, which means that the concentration profile was also stable. Moreover, the small number of interference fringes (eight fringes) denotes a small change of concentration in the observed region, which means the slope of the concentration profile is not too high.

Table 1. Operating Conditions Corresponding to Four Experiments*

Group Experiment	1st I	2nd II	3rd III	4th IV
C_o (kg/m^3)	1.007	9.907	10.02	50.65
$\Delta P\times10^5$ (Pa)	0.98	1.04	1.52	2.28
$J_{water}\times10^6$ (m^3/m^2·s)	3.704	4.327	7.707	14.11
$a\times10^6$ (m^3/m^2·s)	3.215	3.121	5.003	5.265
$b\times10^5$ (s^{-1})	3.1617	2.9531	10.648	16.154
$R_m\times10^{-10}$ (Pa·s/m)	2.63	2.40	1.97	1.62
Ultrafiltration time (s)	2,700	4,320	2,595	2,805
Rest time (pump disconnected) (s)	2,640	3,480	2,160	3,600
Observed area (mm×mm)	1.95×2.60	1.30×1.70	1.30×1.70	1.80×2.40

*Each represents one of the four groups with different conditions.

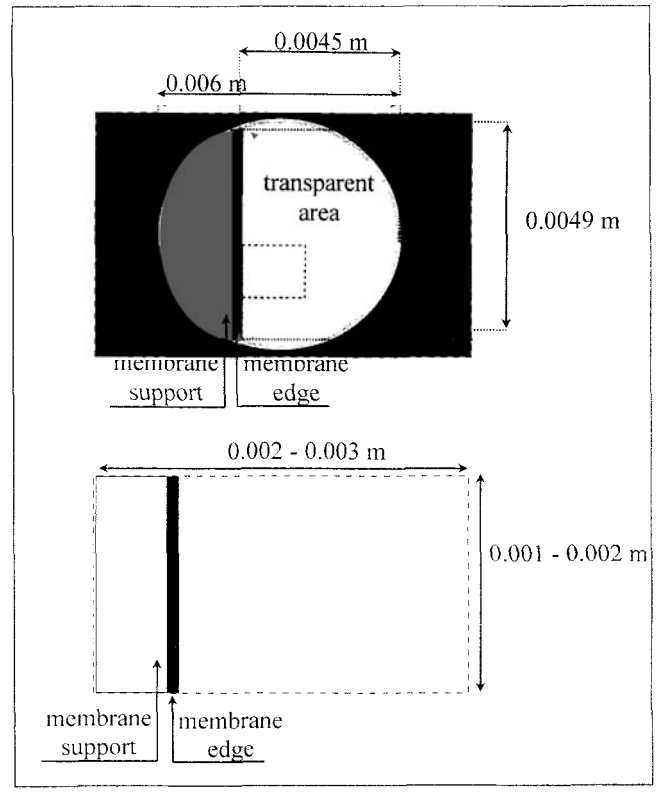

Figure 5. Window visualization: (a) window; (b) observed area in the interferogram.

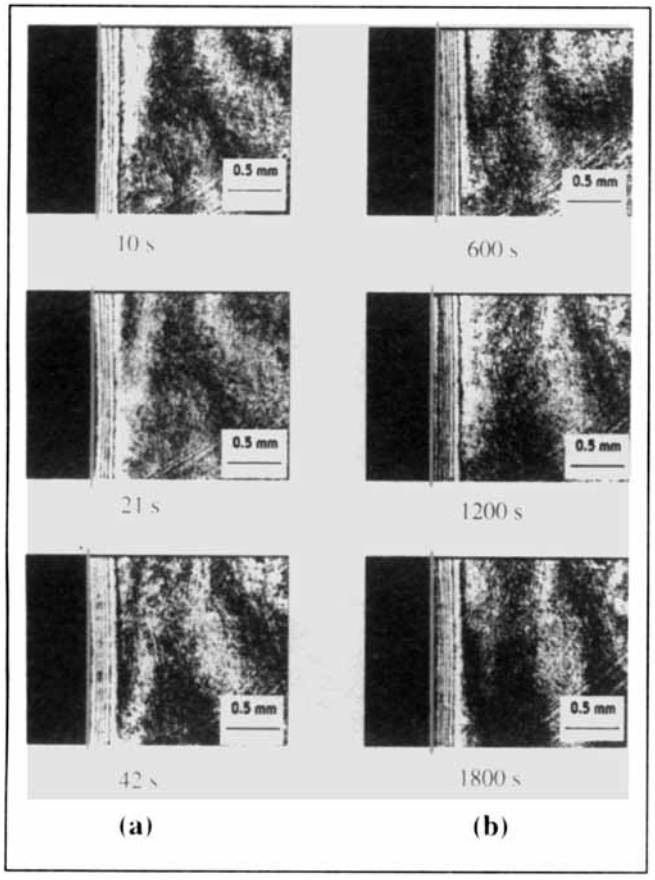

Figure 6. Interferograms belonging to experiment IV ($C_o = 50.65$ kg/m^3 and $\Delta P = 2.28 \times 10^5$ Pa).

Evolution of fringe presence with time (a) at the beginning (10 s, 21 s, and 42 s); (b) with the experiment developed (600, 1,200, and 1,800 s). In general, the membrane position in each interferogram is indicated by means of an additional longer line that extends on each side of the interferogram.

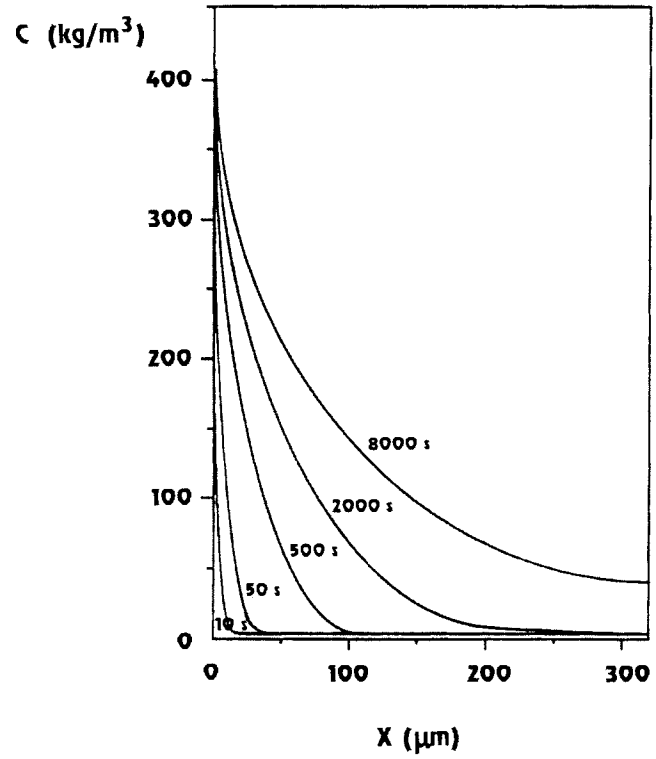

Figure 7. Concentration profiles as a function of time for unstirred dead-end ultrafiltration of BSA.

It was simulated by a model without gel formation (Van den Berg and Smolder, 1990).

This behavior is not expected when an ultrafiltration process is carried out in an unstirred batch module, assuming there is no gel/cake formation. The expected behavior would be that the rejected solute continuously accumulates in proximity to the membrane, causing a continuous increase in the concentration and, therefore, a continuous modification of the concentration profiles. In Figure 7, which is from Van den Berg and Smolders (1990), the theoretically simulated concentration profiles near the membrane interface are shown as a function of time for unstirred dead-end ultrafiltration of BSA ($C_o = 4$ kg/m^3 and $\Delta P = 10^5$ Pa). They employed a model without gel formation. As can be seen, concentrations near the membrane are very high, as are the concentration profile slopes. Moreover, as time goes by, concentration changes take place at points farther away from the membrane. This simulation model predicts that when the concentration gradient is high, a diffusive flow back to the bulk of the feed solution will occur, in such a way that the convective solute flow to the membrane surface will be balanced. In this case, the stabilization of the concentration profiles would be visualized as a great number of narrow interference fringes. The earlier simulation sharply contrasts with our experiments when ultrafiltering BSA, where the number of interference fringes observed was small; the most consistent explanation is to assume that a part of the solutes rejected by the membrane is not in solution, but undergoes a process of coagulation, aggregation–precipitation, and forms the so-called gel layer or filter cake. This filter cake was not evident in Figure 6, possibly due to the effect of pressure, which compacts the protein aggregates. However, the filter cake could be visualized when the pump was switched off, because releasing the pressure caused the cake to relax, allowing a great number of narrow interference fringes to appear. Moreover, thanks to the continuous recording, it was possible to observe additional evidence of the existence of this filter cake: at certain moments, small drops of gelatinous mass trickled down the vertical surface of the membrane, as can be seen for experiment IV in Figure 8. In general, the greater the initial solution concentration (C_o) and transmembrane pressure (ΔP), the easier the observation of the cake became. The drops observed after the pump was switched off could not be confused with air bubbles, which have another appearance and behavior and flow upwards.

All the experiments carried out under the conditions of the first group ($C_o \cong 1$ kg/m^3 and $\Delta P \cong 1 \times 10^5$ Pa) have wider fringes and a smaller number of interference fringes. Furthermore, during the first minutes of these experiments, a widening of the dark zone nearest to the membrane was observed. This dark zone was $0.6–2 \times 10^{-4}$ m wide and was presumably due to a filter cake that was not very compact because of the low ΔP applied. When the pump was stopped and the pressure ceased, the dark zone initially became

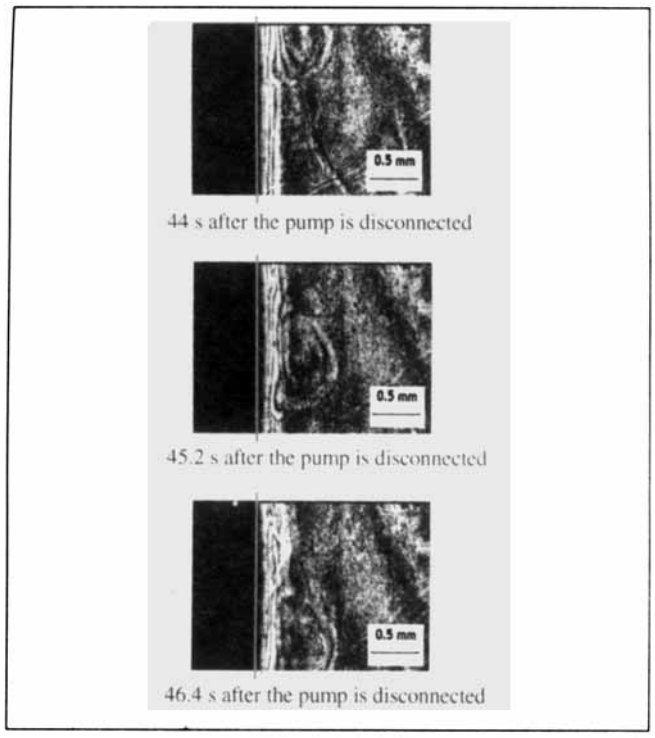

Figure 8. Three consecutive interferograms for experiment IV ($C_o = 50.65$ kg/m^3 and $\Delta P = 2.28 \times 10^5$ Pa), when the pump is switched off.

$t_1 = 44$ s, $t_2 = 45.2$ s, and $t_3 = 46.4$ s after the pump is disconnected. A gel drop sliding above the membrane surface can be seen.

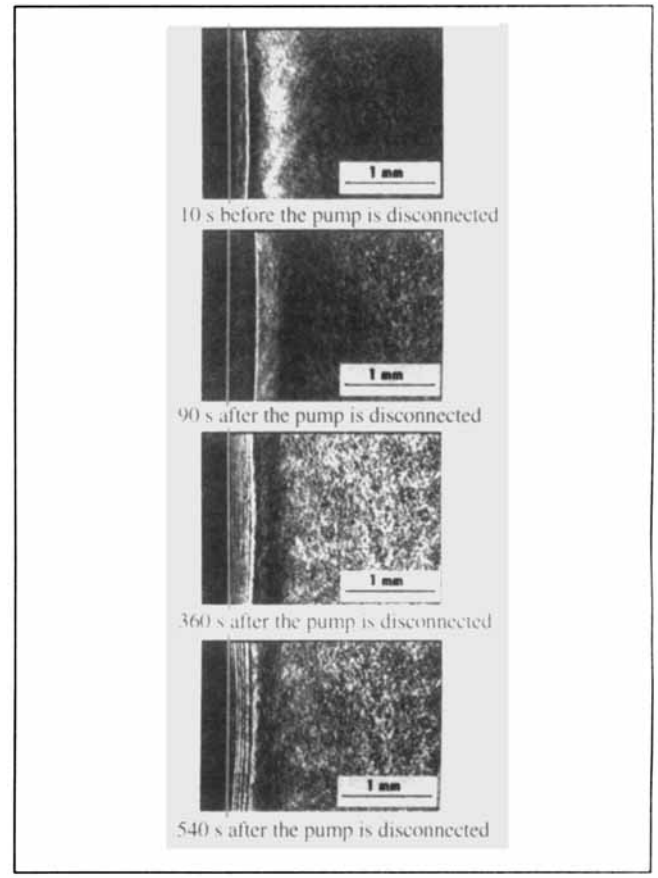

Figure 9. Interferograms belonging to the experiment I ($C_o = 1.007$ kg/m^3 and $\Delta P = 0.98 \times 10^5$ Pa).

$t_1 = 10$ s before the pump is disconnected; $t_2 = 90$ s; $t_3 = 360$ s; and $t_4 = 540$ s after the pump is disconnected.

broader, and then was transformed into a large number of narrow interference fringes. Later, the fringes became more and more separated and finally disappeared (see Figure 9, which corresponds to experiment I). The phenomenon can be explained by the decompression effect of the filter cake and, later, the diffusion of the solute from the membrane surface to the fluid bulk. In this case, when working with small values of C_o and ΔP, no gelatinous drops trickling down the membrane surface were observed. In the other series of experiments, the greater the C_o and ΔP, the thinner the dark zone was. At the same time, it was easier to observe the cake drops (see Figure 10 for experiment II).

Measurement of concentration profiles

Interference fringes that appear in the interferograms are the result of a refractive-index gradient in the vicinity of the membrane due to a concentration gradient. As in BSA aqueous solutions, there exists a relation between refractive index and concentration (Vilker, 1975) and it is possible to obtain the concentration profile from the interference fringes, using the methodology previously explained.

As previously stated, our experiments can be grouped into four categories. Calculation of concentration profiles has been carried out in the experiments with high feed concentration (experiments II, III, and IV), because they lead to interferograms that have narrow and sharp fringes, whereas interferograms corresponding to experiments belonging to the first group do not show the same behavior. Table 2 shows the number of interference fringes, the distance to the membrane for each fringe, and its concentration for three interferograms obtained at 600, 1,200, and 1,800 s, corresponding to the aforementioned experiments. The fringes farthest from the membrane surface (orders number 1 and 2) are broader, and it is more difficult to precisely assign their position because of the difficulty to exactly place where the maximum or the minimum of light intensity is. For experiments II and IV, Figure 11 shows the evolution of the concentration profiles from Table 2; they are very different from those presented by Van den Berg and Smolder (1990) in Figure 7. In this latter figure, a large scope and change in concentration with time can be observed; for example, at 50 μm from the membrane, the concentration changes from almost zero at 50 s to almost 75 kg/m^3 at 500 s, and to almost 150 kg/m^3 at 2000 s. This trend is not the same as in our experiments, in which a small slope can be seen. As was previously indicated, it can be observed that, shortly after switching on the pump, the concentration profiles remain nearly stable during the ultrafiltration process. However, the process is not at steady state because the permeate flux decreases with time as the values of parameter b in Table 1 show. If the steady state has been reached, equation:

$$J \cdot C = -D(\partial C/\partial y) \tag{5}$$

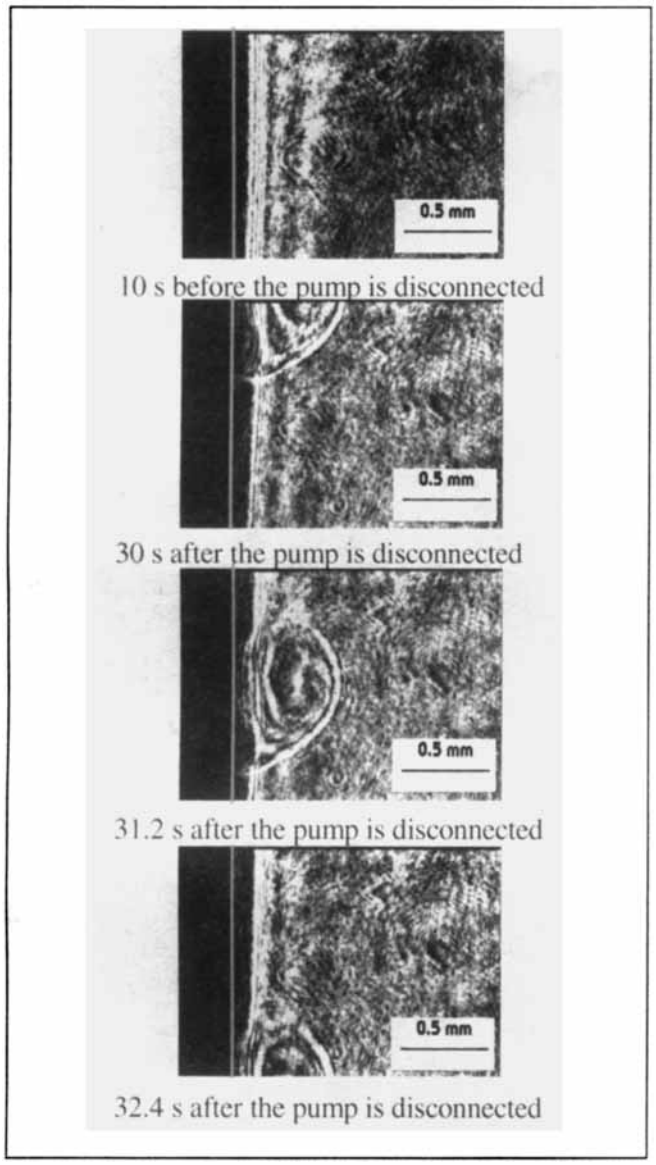

Figure 10. Interferograms belonging to experiment III ($C_o = 10.02$ kg/m^3 and $\Delta P = 1.52 \times 10^5$ Pa).

$t_1 = 10$ s before the pump is disconnected; $t_2 = 30$ s; $t_3 = 31.2$ s; and $t_4 = 32.4$ s after the pump is disconnected. Note a gel drop sliding above the membrane surface.

must be satisfied; that is, the solute convective flux from the solution bulk completely balances the diffusive transport to the bulk due to the concentration gradient.

It is easy to prove, in all the experiments carried out by us, that

$$J \cdot C > - D(\partial C/\partial y), \qquad (6)$$

that is, the convective transport is greater than the diffusive one. The ratio between convective and diffusive fluxes can be expressed by the dimensionless Peclet number ($u\delta/D$), where u, the velocity in the normal direction to the membrane, is numerically equal to J, the volumetric permeate flux, and δ is the concentration boundary-layer thickness. Values of $J \cdot C$ and of $D(\partial C/\partial y)$ at a certain distance from the membrane

Table 2. Concentration Profiles

Fringe Order No.	Interferogram at 600 s y (mm)	at 600 s C (kg/m^3)	at 1,200 s y (mm)	at 1,200 s C (kg/m^3)	at 1,800 s y (mm)	at 1,800 s C (kg/m^3)
Experiment II: $C_o = 9.907$ kg/m^3, $\Delta P = 1.04 \times 10^5$ Pa						
2	0.269	10.22	0.219	10.22	0.313	10.22
3	0.131	10.38	0.163	10.38	0.189	10.38
4	0.106	10.54	0.131	10.54	0.156	10.54
5	0.094	10.70	0.106	10.70	0.131	10.70
6					0.106	10.86
Experiment III: $C_o = 10.025$ kg/m^3, $\Delta P = 1.52 \times 10^5$ Pa						
2	0.293	10.34	0.323	10.34	0.305	10.34
3	0.146	10.50	0.189	10.50	0.171	10.50
4	0.091	10.66	0.116	10.66	0.134	10.66
5	0.073	10.82	0.091	10.82	0.110	10.82
6	0.055	10.98	0.073	10.98	0.085	10.98
7			0.049	11.14	0.061	11.14
8					0.037	11.29
Experiment IV: $C_o = 50.653$ kg/m^3, $\Delta P = 2.29 \times 10^5$ Pa						
1	0.299	50.81				
2	0.173	50.97	0.207	50.97	0.315	50.97
3	0.118	51.13	0.143	51.13	0.166	51.13
4	0.086	51.29	0.104	51.29	0.124	51.29
5	0.055	51.45	0.080	51.45	0.091	51.45
6	0.032	51.60	0.056	51.60	0.066	51.60
7	0.016	51.76	0.040	51.76	0.041	51.76
8			0.016	51.92	0.017	51.92

surface, as well as of the Peclet number, have been calculated for several interferograms corresponding to the aforementioned experiments and are presented in Table 3. Thickness δ has been estimated as about 320 μm from the position of the further fringe. The value of the BSA solution diffusion coefficient used in these calculations is that mentioned in the literature: 7×10^{-11} m^2/s (Vilker, 1981b). In the literature other diffusion coefficient values, ranging from 1.5 to 9×10^{-11} m^2/s (Probstein et al., 1978; Arunyawongsakorn et al., 1985; and Gill et al., 1988), can be found. However, as far as the calculation of Table 3 is concerned, given that the dif-

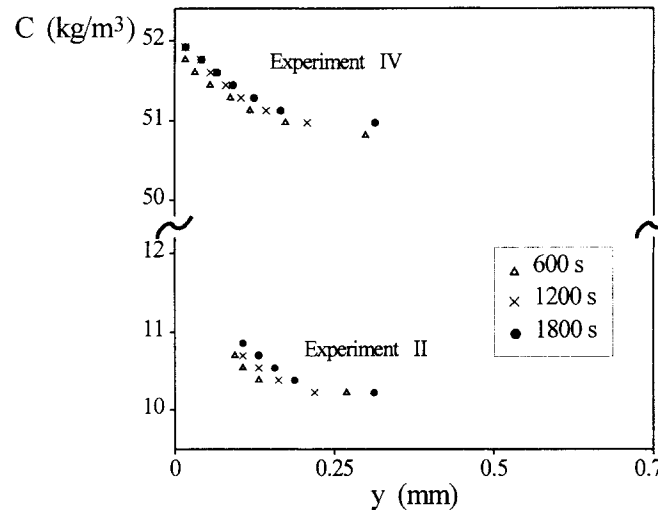

Figure 11. Concentration profiles at different times.

Experiment II: $C_o = 9.907$ kg/m^3 and $\Delta P = 1.04 \times 10^5$ Pa; experiment IV: $C_o = 50.65$ kg/m^3 and $\Delta P = 2.28 \times 10^5$ Pa.

Table 3. Calculation of Convective and Diffusive Fluxes

Exp.	Time (s)	Position (mm)	C (kg/m^3)	$J \cdot C \times 10^5$ (kg/s·m^2)	$-D(\Delta C/\Delta y) \times 10^7$ (kg/s·m^2)	Pe
II	600	0.12	10.4	3.19	4.55	14
	1,200	0.12	10.6	3.19	4.90	14
	1,800	0.12	10.7	3.17	5.60	13
III	600	0.07	10.8	5.07	5.60	22
	1,200	0.07	10.9	4.80	5.95	20
	1,800	0.07	11.0	4.54	6.30	19
IV	600	0.05	51.5	24.6	4.90	22
	1,200	0.05	51.6	22.4	5.25	20
	1,800	0.05	51.7	20.3	5.60	18

fusive flux is around 100 times less than the convective flux, the use of any value of the diffusion coefficient in the range between 1.5 and 9×10^{-11} m^2/s would not alter the conclusions mentioned earlier.

The convective flux of solute, $J \cdot C$ is about 10^{-5} kg/(s·m^2), whereas the diffusive flux, $-D(\partial C/\partial y)$, is clearly less, about 10^{-7} kg/(s·m^2). The difference between convective and diffusive fluxes, $s = J \cdot C - [-D(\partial C/\partial y)]$, is retained by the membrane, but it is not used to increase the concentration. According to the experimental data from the visualization process, this solute flux, s, separates from the solution and forms a more or less compact gel layer on the membrane surface. The process in Figure 12 shows the solute balance in a control volume near the membrane surface.

The cake layer behaves as a sink in such a way that the solute integrates with the gel and does not increase the concentration. As a result of this, the state of the system can be considered as "pseudo-steady-state" because, although the concentration profile remains constant with time, the amount of solute accumulated in the cake increases and, in some way, the hydraulic resistance offered by the cake slightly increases, thus causing the permeate flux (J) to decrease with time. Figure 13 shows the evolution of the nondimensional flux, J/J_{water}, in the three experiments shown in Table 3. As can be seen, the permeated flux (J) suffers a considerable reduction at the beginning of the ultrafiltration process (0.75, 0.65, and 0.37 for experiments II, III, and IV, respectively) compared

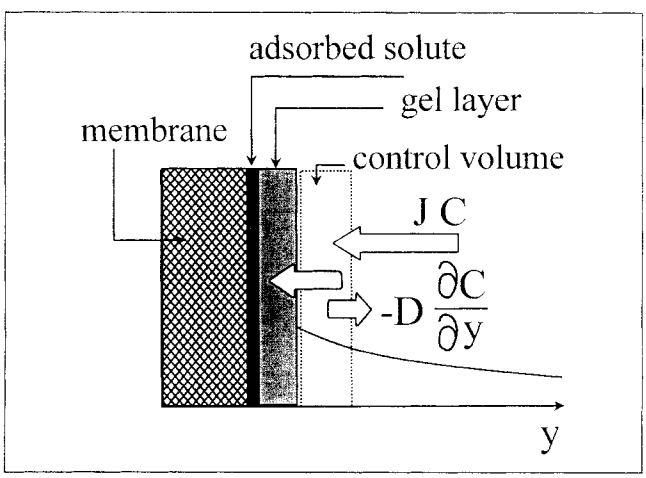

Figure 12. Solute balance in a control volume near the membrane surface.

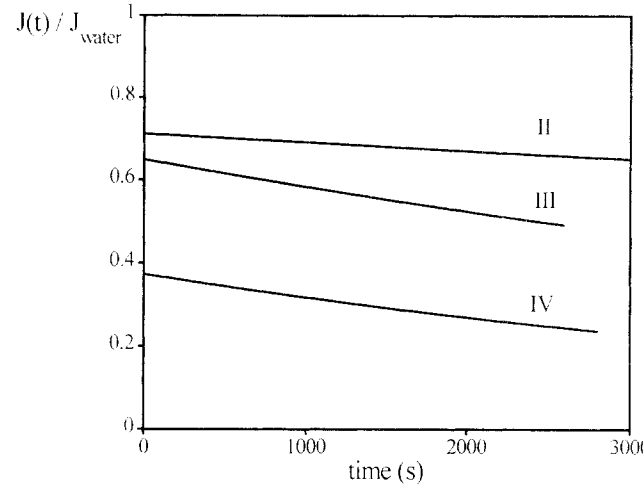

Figure 13. Evolution of the dimensionless flux (J/J_{water}).

Experiment II: $C_o = 9.907$ kg/m^3 and $\Delta P = 1.04 \times 10^5$ Pa; experiment III: $C_o = 10.02$ kg/m^3 and $\Delta P = 1.52 \times 10^5$ Pa; experiment IV: $C_o = 50.65$ kg/m^3 and $\Delta P = 2.28 \times 10^5$ Pa.

to the pure-water flux (J_{water}). Similar behavior has been reported by Matthiasson (1984).

At this point it is convenient to observe that, according to the literature (Matthiasson et al., 1983; Aimar et al., 1986), polysulfone membranes have a large capacity to adsorb the BSA proteins, even when the experiment is carried out in static conditions; that is, when the membrane is simply put in contact with a BSA protein solution. This fact also has been experimentally confirmed in our laboratory (Fernández, 1996). The amount of solute adsorbed is very high and is more than that corresponding to only one monolayer. The reason for this is the large interaction between the polysulfone membrane and the BSA proteins (Matthiasson et al., 1983). In our case, before each experiment the membrane (polysulfone) is put in contact with the BSA solution for 40–60 min without pressure. In this way, the adsorption phenomenon takes place and the adsorption equilibrium is reached before the ultrafiltration process starts.

The layer of adsorbed solute implies hydraulic resistance (R_a) added to the membrane resistance with water (R_m). This could therefore explain the large reduction in the permeated flux compared to the flux with pure water observed in Figure 13. On the other hand, as can be noted in Figure 13, the evolution of flux, which decreases with time, must be attributed to the filter-cake build-up and not to the influence of osmotic pressure because, as we have experimentally seen from holographic interferometry, concentration does not increase too much. As is known, the driving force correction with osmotic pressure effect is very important in the case of reverse osmosis since, on the one hand, the osmotic pressure of inorganic salts is very high even at low concentrations and, on the other hand, the concentration polarization profiles in reverse osmosis show a large slope, since very soluble rejected solutes, adjacent to the membrane, are maintained in solution and reach high concentrations. In ultrafiltration, however, the solute is a macromolecule with a high molecular weight. Therefore, macromolecule solutions with weight percentage concentrations equivalent to those of salts have an osmotic pressure that is approximately 1,000 times less (the

ratio between their molecular weights, macromolecule/salt). Furthermore, due to protein deposition on the membrane surface, a filter cake develops, so that the concentration in solution near the membrane surface does not reach a high value.

Before we can attribute the decline of flux to the increase in osmotic pressure, the concentration profiles should vary with time, making the slope greater. In our experiments, profiles were stable with time. The solute retained by the membrane was accumulated in the filter cake but not in the solution. Consequently, the decrease in flux cannot be attributed to a greater osmotic pressure, but to the increase in the specific resistance of the filter cake. These considerations are supported by the literature. Bowen and Williams (1996), Bowen and Ahmad (1997), Nakakura et al. (1997), and Mukai et al. (1997), show experimental evidence of filter-cake formation during BSA ultrafiltration, using the filter-cake theory to interpret their results and disregarding the use of the osmotic pressure model. The gel layer or filter-cake build-up near the membrane surface is formed during the dynamic process of ultrafiltration, and is weakly bound to the membrane. Its nature is therefore different than that of the solute adsorbed in a static way, which occurs when the BSA solution comes in contact with the membrane. The weakness of this boundary was visually confirmed when the pump was stopped: a mass of cake was released and trickled down the membrane surface (Figures 8 and 10).

Although some authors (Vilker et al., 1981b; Boulanouar et al., 1996) have dismissed the build-up of a gel layer during the ultrafiltration of BSA if concentration does not reach the solubility limit (580 kg/m^3), other authors (Matthiasson, 1984; Fernández, 1996) consider that interactions between the macrosolute and the membrane, at concentrations under this limit, may cause the formation of this gel layer or filter cake. It can also be deduced from these different studies that the nature of the membrane is a deciding factor in the outcome of ultrafiltration. Vilker et al. (1981b) worked with a cellulosic membrane, a material without noticeable solute–membrane interactions. Boulanouar et al. (1996) worked with a membrane (Spectra/Por flat disc, C type) also without solute–membrane interactions. Matthiasson et al. (1983) studied the water fluxes obtained after an hour of contact between different concentrations of BSA solutions (0.4 g/100 mL–50 g/100 mL) and different membranes (polyamide, polysulfone, and cellulose acetate). These authors were able to deduce from their adsorption (no ultrafiltration) results that *the reduction in flux for the hydrophobic polysulfone and polyamide membranes is much higher than that for the hydrophilic cellulose acetate membrane*, that is to say, it is reasonable that Vilker et al. as well as Boulanouar et al. did not find experimental evidence of gel formation, and so they do not have to consider gel-layer formation in their theories. As an example, Matthiasson et al. (1983) found that, even with low concentrations (1 to 10 kg/m^3), large amounts of solute were adsorbed (20–40 mg/m^2) when working with a polysulfone membrane (the same membrane material we used in our experiment). When higher concentrations were used, the amount of solute bounded to the membrane increased considerably, an accumulation process that looked more like some kind of surface coagulation process than a surface adsorption process. These authors considered that the molecular interactions and protein aggregation phenomena that occur when concentration increases could favor the adsorption phenomenon, and added that "the so-called gel layer is not formed as soon as the concentration at the wall has reached the saturation concentration of the protein (around 58 g/100 mL) but rather gradually over the whole concentration range." In the case of ultrafiltration, the gel-layer or filter-cake formation can take place as a consequence of the pressure increase and the compactness of corresponding protein aggregates. Using an unstirred batch module, Matthiasson (1984) found a secondary hydraulic resistance in addition to the one caused by the membrane itself and the adsorbed layer. This secondary resistance did not have the same irreversible character as resistance due to the adsorbed layer, because it disappeared when the protein solution was replaced by pure buffer solutions. Furthermore, he added that "this secondary resistance is due to protein not as tightly bound to the surface as the adsorbed layer," which agrees with the results of our visualization experiments.

Several experimental works have recently been published that confirm the formation of a filter cake in operating conditions similar to those of our experiments: dead-end (zero cross-flow) ultrafiltration cell, BSA solution feed, and polysulfone membranes. Bowen and Ahmad (1997) used electric-field pulses to release the filter cake for collection. The majority of the experiments were carried out with feed concentrations of 1 g/L and $\Delta P = 1$ bar. In the operation of the filtration cell, a valve on the feed side of the membrane module opened automatically after the application of the electric-field pulse to allow collection of the released cake. Pressure was maintained during the process, and the volume discharged was equivalent to the volume of the feed chamber. Nakakura et al. (1997) investigated experimentally the dynamic ultrafiltration process of BSA solutions by measuring electrical conductivity within the filter cake. Pairs of platinum-wire electrodes were employed to measure the formation process of the filter cake on the membrane surface. The filter cake formed from protein solutes behaves in the same way as highly compressible cakes. The experimental results for BSA and soy protein solutions coincide favorably with the calculated results based on compressible filtration theory. Mukai et al. (1997) obtained the properties—average porosity ϵ_{av} and average specific filtration resistance α_{av}—of the filter cake formed on the retentive membrane in dead-end ultrafiltration of BSA solutions. The average porosity of the filter cake was measured by a modified ultrafiltration cell. The filtration area was suddenly reduced at a distance of 0.4 mm from the membrane surface in such a way that when the cake surface reached a width of 0.4 mm, the reciprocal filtration rate increased sharply due to the change in filtration area. This change allowed the critical volume of filtration to be obtained. The experimental results confirming the existence of filter-cake formation obtained by the aforementioned authors agree with our visualization experiments.

Conclusions

Continuous observation of the concentration polarization phenomenon during the ultrafiltration of protein BSA, using a membrane made of polyethersulfone, was achieved by means of holographic interferometry. The results show that during the first few seconds, a determinate number of inter-

ference fringes appear. Later on, this number remains stable. The concentration profiles obtained from the interferometric information reveal a low level of concentration, a fact that agrees with the filter-cake present. Furthermore, when the pump is stopped, a large quantity of gelatinous material appears, sliding down the membrane surface. These results and those of recent literature (Nakakura et al., 1997; Bowen and Ahmad, 1997; Mukai et al., 1997) agree with the conclusion that, with BSA solution and with a polyethersulfone membrane, a filter cake forms on the membrane even when the wall concentration is well below the value for gel formation, and therefore must be considered when designing a model.

Acknowledgments

This research was sponsored partially by the C.A.I.C.yT. PS 88-0063 (Ministerio de Educación y Ciencia). Ms. M. J. Fernández-Torres was awarded a grant by the Consellería d'Educació i Ciencia (Generalitat Valenciana). Holographic interferometry equipment was financed by the Consellería d'Educació i Ciencia (Generalitat Valenciana).

Literature Cited

Aimar, P., S. Baklouti, and V. Sánchez, "Membrane-Solute Interactions: Influence on Pure Solvent Transfer During Ultrafiltration," *J. Memb. Sci.*, **26**, 207 (1986).

Arunyawongsakorn, U., C. S. Johnson, Jr., and D. A. Gabriel, "Tracer Diffusion Coefficients of Proteins by Means of Holographic Relaxation Spectroscopy: Application to Bovine Serum Albumin," *Anal. Biochem.*, **146**(1), 265 (1985).

Boulanouar, I., S. Nicolas, and B. Bariou, "Ultrafiltration and Reverse Osmosis in Unstirred Batch Cell of Charged Solutes (Protein, Salts) with Total Retention," *Desalination*, **104**, 83 (1996).

Bowen, W. R., and A. L. Ahmad, "Pulsed Electrophoresis Filter-Cake Release in Dead-End Membrane Processes," *AIChE J.*, **43**(4), 959 (1997).

Bowen, W. R., and F. Jenner, "Dynamic Ultrafiltration Model for Charged Colloidal Dispersions: A Wigner-Seitz Cell Approach," *Chem. Eng. Sci.*, **50**, 1701 (1995).

Bowen, W. R., and P. M. Williams, "Dynamic Ultrafiltration Model for Proteins: A Colloidal Interaction Approach," *Biotechnol. Bioeng.*, **50**, 125 (1996).

Bradford, N. N., "A Rapid and Sensitive Method for the Quantitation of Microgram Quantities of Protein Utilizing the Principle of Protein-Dye Binding," *Anal. Biochem.*, **72**(1/2), 248 (1976).

Clifton, M., and V. Sánchez, "Holographic Interferometry Applied to the Measurement of Boundary Layers in Electrodialysis and Ultrafiltration," *Optics and Photonics Applied to Medicine*, Vol. 211, Soc. Photo-Opt. Instrum. Eng., p. 111 (1979).

Ethier, C. R., and D. C. Lin, "Refractometric Measurements of Polarized Layer Structure: Studies of Hyaluronic Acid Ultrafiltration," *J. Memb. Sci.*, **68**, 249 (1992).

Fernández-Torres, M. J., "Estudio de la Ultrafiltración de Disoluciones de Proteína BSA Mediante Interferometría Holográfica Microscópica. Revisión Crítica de los Modelos de Simulación a Partir de los Datos Obtenidos por Visualización de la Capa de Polarización," PhD Thesis, Universidad de Alicante, Alicante, Spain (1996).

Fernández-Sempere, J., F. Ruiz-Beviá, J. Colom-Valiente, and F. Más-Pérez, "Determination of Diffusion Coefficients of Glycols," *J. Chem. Eng. Data*, **41**, 47 (1996).

Gill, W. N., D. E. Wiley, C. J. D. Fell, and A. G. Fane, "Effect of Viscosity on Concentration Polarization in Ultrafiltration," *AIChE J.*, **34**(9), 1563 (1988).

Gowman, L. M., and C. R. Ethier, "Concentration and Concentration Gradient Measurements in an Ultrafiltration Concentration Polarization Layer. Part I: A Laser-Based Refractometric Experimental Technique," *J. Memb. Sci.*, **131**, 95 (1997a).

Gowman, L. M., and C. R. Ethier, "Concentration and Concentration Gradient Measurements in an Ultrafiltration Concentration Polarization Layer. Part II: Application to Hyaluronan," *J. Memb. Sci.*, **131**, 107 (1997b).

Hendricks, T. J., and F. A. Williams, "Diffusion-Layer Structure in Reverse Osmosis Channel Flow," *Desalination*, **9**, 155 (1971).

Johnson, A. R., "Experimental Investigation of Polarization Effects in Reverse Osmosis," *AIChE J.*, **20**(5), 966 (1974).

Kozinski, A. A., and E. N. Lightfoot, "Protein Ultrafiltration: A General Example of Boundary Layer Filtration," *AIChE J.*, **18**(5), 1030 (1972).

Liu, M. K., and F. A. Williams, "Concentration Polarization in an Unstirred Batch Cell: Measurements and Comparison with Theory," *Int. J. Heat Mass Transfer*, **13**, 1441 (1970).

MacRitchie, F., "Effects of Temperature on Dissolution and Precipitation of Proteins and Polyamino Acids," *J. Colloid Interf. Sci.*, **45**, 235 (1973).

Mahlab, D., N. B. Yosef, and G. Belfort, "Concentration Polarization Profile for Dissolved Species in Unstirred Batch Hyperfiltration (Reverse Osmosis): II. Transient Case," *Desalination*, **24**, 297 (1978).

Matthiasson, E., "Macromolecular Adsorption and Fouling in Ultrafiltration and Their Relationships to Concentration Polarisation," PhD Thesis, Lund Univ., Lund, Sweden (1984).

Matthiasson, E., B. Hallström, and B. Sivik, "Adsorption Phenomena in Fouling UF-Membranes," *Proc. Int. Cong. of Eng. and Food*, Dublin, Ireland (1983).

McDonogh, R. M., H. Bauser, N. Stroh, and U. Grauschopf, "Experimental in situ Measurement of Concentration Polarisation During Ultra- and Micro-Filtration of Bovine Serum Albumin and Dextran Blue Solutions," *J. Memb. Sci.*, **104**, 51 (1995).

McDonogh, R. M., H. Strathmann, H. Bauser, N. Stroh, and E. Walitza, "Identification of Controlling Mechanisms in Ultrafiltration Based on Direct Measurements of the Polarised Layer," *Récents Prog. Génie Procedes*, **6**(22), 233 (1992).

Mukai, Y., E. Iritani, and T. Murase, "Effect of Protein Charge on Cake Properties in Dead-End Ultrafiltration of Protein Solutions," *J. Memb. Sci.*, **137**, 271 (1997).

Nabe, A., E. Staude, and G. Belfort, "Surface Modification of Polysulfone Ultrafiltration Membranes and Fouling by BSA Solutions," *J. Memb. Sci.*, **133**, 57 (1997).

Nakakura, H., A. Yamashita, M. Sambuichi, and K. Osasa, "Electrical Conductivity Measurement of Filter Cake in Dead-End Ultrafiltration of Protein Solution," *J. Chem. Eng. Jpn.*, **30**(6), 1020 (1997).

Noble, R. D., and S. A. Stern, *Membrane Separations Technology. Principles and Applications*, Chap. 2, Elsevier, Amsterdam (1995).

Probstein, R. F., J. S. Shen, and W. F. Leung, "Ultrafiltration of Macromolecular Solutions at High Polarization in Laminar Channel Flow," *Desalination*, **24**, 1 (1978).

Ruíz-Beviá, F., A. Celdrán-Mallol, C. Santos-García, and J. Fernández-Sempere, "Liquid Diffusion Measurement by Holographic Interferometry," *Can. J. Chem. Eng.*, **63**, 765 (1985a).

Ruíz-Beviá, F., A. Celdrán-Mallol, C. Santos-García, and J. Fernández-Sempere, "Holographic Interferometric Study of Free-Diffusion: A New Mathematical Treatment," *Appl. Opt.*, **24**(10), 1481 (1985b).

Ruíz-Beviá, F., J. Fernández-Sempere, and J. Colom-Valiente, "Diffusivity Measurement in Calcium Alginate Gel by Holographic Interferometry," *AIChE J.*, **35**(11), 1855 (1989).

Ruíz-Beviá, F., J. Fernández-Sempere, and N. Boluda-Botella, "Variation of Phosphoric Acid Diffusion Coefficient with Concentration," *AIChE J.*, **41**, 185 (1995).

Van den Berg, G. B., and C. A. Smolders, "Flux Decline in Ultrafiltration Processes," *Desalination*, **77**, 101 (1990).

Vest, C. M., *Holographic Interferometry*, Wiley, New York (1979).

Vilker, V. L., "The Ultrafiltration of Biological Macromolecules," PhD Thesis, Massachusetts Inst. of Technol., Cambridge (1975).

Vilker, V. L., C. K. Colton, K. A. Smith, and D. L. Green, "Concentration Polarisation in Protein Ultrafiltration: I. An Optical Shadowgraph Technique for Measuring Concentration Profiles Near a Solution-Membrane Interface," *AIChE J.*, **27**, 632 (1981a).

Vilker, V. L., C. K. Colton, K. A. Smith, and D. L. Green, "Concentration Polarisation in Protein Ultrafiltration: II. Theoretical and Experimental Study of Albumin Ultrafiltered in an Unstirred Cell," *AIChE J.*, **27**, 637 (1981b).

Manuscript received Apr. 8, 1997, and revision received Apr. 2, 1998.